RSC Advances

ROYAL SOCIETY OF CHEMISTRY

www.rsc.org/advances

Journal Name

ARTICLE

Improving hemocompatibility of polypropylene via surface-initiated atom transfer radical polymerization for covalently coupling BSA

Chunming Li[ab], Jing Jin*[a], Jingchuan Liu[a], Xiaodong Xu[c], Jinghua Yin*[a],

Bovine serum albumin (BSA) modified polypropylene (PP) was fabricated via surface-initiated atom transfer radical polymerization (SI-ATRP) of poly (ethylene glycol) methacrylate (PEGMA) and glycidyl methacrylate (GMA). Kinetics study revealed an approximately linear increase in graft density of the functional brushes with polymerization time. Attenuated total reflectance Fourier transform infrared spectroscopy, X-ray photoelectron spectroscopy confirmed that comonomers and BSA were successfully immobilized onto PP film. The hydrophilicity of PP was improved by modification with PEGMA and GMA. The balance between the inhibition of BSA adsorption by PEGMA and the covalently immobilization of BSA by GMA through the ring-open reaction of the epoxy group resulted in the moderate fluorescence intensity of FITC-BSA immobilized PP-g-P (PEGMA-co-GMA). The hemolysis test showed that BSA could decrease the hemolysis rate. Red blood cell membrane maximal stress can be reduced by the inertness of BSA as well as the repulsion caused by its electrostatic interactions. Whole blood cell attachment test showed that BSA molecules weakened the interaction between blood cells and the PP surface. Therefore, the immobilization of BSA on PP film is an effective approach for improving the hemocompatibility of PP.

1. Introduction

Thrombus formation and hemolysis are two major complications affecting the use of blood-contacting medical devices[1, 2]. Hemolysis represents the rupture of red blood cell (RBC) with the direct release of hemoglobin (Hb) into the suspending medium, which may lead to organ failure and patient death during blood transfusion[3]. Several factors cause hemolysis, including shear stress, turbulence, temperature, and biomaterial surface-induced hemolysis during storage and transportation in blood bags. Two problems on hemolysis must be addressed. First, the mechanism of hemolysis is unknown. The accumulation of lipid peroxidation of the RBC membrane causes membrane damaged during storage and transport[4]. This condition could decrease membrane integrity and flexibility, and lead to hemolysis. The gradual release of Hb and its all-or-none alternative have been proposed, but neither has gained wide acceptance[5]. Second, little information is available on biomaterial surface induced-hemolysis during processing, storage, transfusion, and transport.

Polypropylene (PP) is one of the widely used materials in blood-contacting medical devices, owing to its non-toxic and excellent mechanical properties. Improving the hydrophilicity and hemocompatibility of PP is imperative for preparing PP-based biomaterials. Previous studies show that the anticoagulant performance of PP can be improved[6-8]. Protein modified PP as biomaterial has been in-depth researched by Genzer's group[9, 10]. However, the hemolytic property of PP and its use as blood storage bags has not gained widespread concern. To fabricate antihemolytic PP, the suitability of its surface anticoagulant performance should first be confirmed. Surface-initiated atom transfer radical polymerization (SI-ATRP) is one of the classical and popular methods used for PP surface modification. The functional groups of polymer brushes used for biomolecule immobilization include epoxide, carboxylic acid, hydroxyl, aldehyde, and amine group. Glycidyl methacrylate (GMA) bears a reactive epoxide group, which can react with amino-, sulfhydryl-, hydroxyl-, and carboxyl group of biomolecules to form stable covalent bonds. Biomaterials grafted with GMA have been used for covalently coupling biomolecules such as proteins and enzymes[11, 12]. However, this coupling will result non-specific protein absorption due to hydrophobic property of P (GMA). Poly (ethylene glycol) (PEG)-based polymers have been recognized as non-fouling coatings for decades[13-15]. Polymer brushes containing a high density of PEG side chains have been successfully synthesized via surface-initiated atom transfer radical polymerization (SI-ATRP) to prevent non-specific protein adsorption[16, 17].

Serum albumin is a naturally occurring and highly specific functional biopolymer, which maintains the colloid osmotic pressure and improves blood compatibility of materials[18-20]. G. Barshtein et al. investigated the effect of albumin on the hemolytic activity of polystyrene nanoparticles[21]. They have proved that the hemolytic effect of nanoparticle is strongly modulated by albumin concentration in the medium. P. Khullar et al. have also found that albumin can improve the hemolytic effect of gold nanoparticles[22]. They concluded that BSA-conjugated nanoparticles can have little hemolysis and no cytotoxicity. Although a number of studies on albumin improving the hemolysis of RBC have been reported, few studies have been concerned with the immobilizing the albumin onto the polymer surface and the hemolytic effect of the BSA modified films.

In this study, SI-ATRP of PEG methacrylate (PEGMA) and GMA is performed, followed by immobilization of BSA with epoxide group of P (GMA). This mixture of PEG-rich monomers and epoxy-containing GMA monomers allows us to control the non-fouling ability as well as BSA conjugation sites[23-25]. The kinetics of surface polymerization and the structure of polymer brushes are studied by attenuated total reflectance Fourier transform infrared spectroscopy (ATR-FTIR) and X-ray photoelectron spectroscopy (XPS). The wettability of surfaces is assessed by static water contact-angle measurements. The immobilization of BSA onto PP surface with different pH solution condition is also investigated and confirmed by XPS and confocal laser scanning microscopy (CLSM). Antihemolytic property evaluation including hemolysis rate and whole blood adhesion tests are performed to investigate the interaction between RBCs and the modified surface.

2. Experimental

2.1 Materials

Polypropylene (GM1600E) was obtained from Shanghai Petrochemical Company. The polypropylene granules were extruded into films. The PP films were cut into square of 2 cm × 2 cm in size. Poly (ethylene glycol) methacrylate (PEGMA, M_n=360), glycidyl methacrylate(GMA), 2,2'-byridine (Bpy), copper(I) chloride (CuCl), copper(II) chloride (CuCl$_2$), Bovine serum albumin (BSA), Fibrinogen (Fib) were purchased from Sigma-Aldrich chemical Co. PEGMA and GMA were passed through neutral aluminum oxide column to remove the inhibitor before use. 4-(chloromethyl) phenyltrichlorosilane (CPTS) was obtained from J&K Chemical Ltd. Phosphate-buffered saline (PBS, 0.01 M phosphate buffer, pH 7.4) that was used for protein adsorption, platelet adhesion and immobilization of BSA experiment was prepared freshly. Water in toluene was removed by reaction with metallic sodium. The other solvents and reagents were AR grade and used without further purification.

2.2 Surface-Initiated ATRP of PEGMA and GMA on PP Surface

PP films were washed by acetone for 12 h and cleaned with acetone for 30 min in an ultrasonic water bath. The films were dried under vacuum for 24 h at room temperature before use. Next, the oxygen plasma treatment was conducted using DT-03 plasma apparatus (Suzhou Omega Technology Co., Ltd.) for 120 s. The pre-treated films were immersed in a 3 % (*v/v*) toluene solution of CPTS for 2 h. After that, the films were isolated and ultrasonically washed with chloroform (3 × 20 mL), acetone (2 × 20 mL), ethanol (4 × 20 mL), and, finally, water, in that order. They were then dried in a clean vacuum oven at 70℃ for 20 min[26].

The SI-ATRP was prepared by mixing DI water (4 mL), methanol (4 mL), PEGMA (8 mL), and GMA (400 *μ*L). After bubbling the solution with pure Argon for 15 min, Bpy, CuCl$_2$ and CuCl were dissolved in the monomer solution. The initiator-loaded PP films were placed into the reaction solution. Before polymerization, the flasks were degassed three cycles and backfilled with Argon[27, 28]. The reaction flasks were sealed and kept in a 40℃ oil bath for a predetermined period of time. After the reaction, the PP films with surface grafted PEGMA and GMA were removed from the reaction mixture and washed thoroughly with excess amount of ethanol and water for about 24 h to ensure the complete removal of the adhered and physically adsorbed non-grafted components, if any. The films were dried by pumping under reduced pressure for about 12 h. In this study, the ratio of [PEGMA]: [CuCl]: [CuCl$_2$]: [Bpy] was controlled at 100:1:0.2:2. The molar ratio of PEGMA and GMA used for BSA immobilization was 8:1[23]. The SI-ATRP of different molar ration of PEGMA and GMA was also prepared. The reaction system was prepared in 50% (V/V) methanol. Grafting density of the film was calculated as follows:

$$GD = \frac{W_m - W_0}{S}$$

Where W_0 and W_m are the masses of PP-CPTS and modified PP film, respectively; S is the area of film.

2.3 Protein Immobilization

The abundant amount amino groups of BSA were expected to react readily and irreversibly with the reactive epoxide group of the PP-g-P(PEGMA-*co*-GMA) films. The films were transferred to 10 mL of 0.1 M PBS containing 10 mg/mL BSA or 200 μL 0.2 mg/mL FITC-BSA. The immobilization reaction was allowed to proceed at 37℃ for 3 days. After the reaction period, adsorbed BSA and FITC-BSA were rinsed by PBS for 24 h at room temperature on the shaker, and then washed by an aqueous solution of 1.0 wt. % sodium dodecyl sulfate (SDS) for 5 min in an ultrasonic water bath, followed by ultra-pure water for five times. The FITC-BSA was kept away from light of whole process. In order to check the influence of the buffers pH on the immobilization amount, BSA in PBS buffers with different pH at 2.5 and 4.7 was also applied. The fluorescence intensities of immobilized BSA were determined by confocal laser scanning microscopy (CARL ZEISS LSM 700).

2.4 Surface Characterization

The surface chemical structure of the modified PP films was analyzed by Fourier transform infrared spectroscopy (FTIR, BRUKER Vertex 70) with an ATR unit (Attenuated Total Reflection crystal, 45°) at a resolution of 4 cm^{-1} for 32 scans. In order to visualize the surface functionalization of PP, high-resolution FT-IR microscopy was applied using FT-IR Imaging system of PE (American) (Fig. S2). The chemical composition of modified PP films were characterized by X-ray photoelectron spectroscopy (XPS, VG Scientific ESCA MK II Thermo Avantage V 3.20 analyzer) with Al/K (hν = 1486.6 eV) anode mono-X-ray source. All the samples were completely vacuum dried prior to use. The releasing angle of the photoelectron for each atom was fixed at 90°. Surface spectra were collected over a range of 0-1200 eV and high-resolution spectra of C1s, N1s and O1s regions were collected. The atomic concentrations of the elements were calculated by their corresponding peak areas. Atomic force microscopy (AFM) in tapping mode was carried out on a SPA300HV with a SPI 3800 controller (Seiko Instruments Industry, Japan). The root-mean-square (RMS) roughness was evaluated directly from AFM images.

The static water contact angles of neat and modified PP films were measured on a drop shape analysis instrument (DSA 100, Kruss GmbH, Hamburg, Germany) by placing 2 μL of distilled water on the surfaces at room temperature. The contact angles were calculated by the instrument using Young-Laplace methods. The reported data were the mean values measured with three samples. The value of each film was obtained by averaging the contact angle for six surface locations.

2.5 Antihemolytic properties

HEMOLYSIS RATE TEST

Fresh blood collected from a healthy rabbit was mixed immediately with a 3.8 wt.% solution of sodium citrate at a dilution ration of 9:1. (The experiments were carried out in accordance with the guidelines issued by the Ethical Committee of the Chinese Academy of Sciences) Erythrocytes were separated from plasma and lymphocytes by centrifugation (3000 g, 5 min) at 4℃, washed three times with normal saline and suspended in normal saline at . Erythrocytes were used immediately after isolation. Neat and modified PP films were equilibrated in normal saline for 60 min at 37℃ and then immersed in 2 mL erythrocytes normal saline suspensions. The samples were incubated for certain time at 37℃. Positive and negative controls were produced by adding 0.2 mL of erythrocytes to 4 mL of distilled water and saline water, respectively. After incubation, the suspensions were centrifuged (3000 g, 5 min). Optical density of the supernatant was measured at 541 nm. The hemolysis rate of modified PP with different ratio of PEGMA and GMA was also investigated (Fig. S3). The percent hemolysis was calculated as follows:

$$hemolysis(\%) = \left[\left(OD_{sam} \text{-} OD_{neg} \right) \Big/ \left(OD_{pos} \text{-} OD_{neg} \right) \right] \times 100$$

Where OD_{sam}, OD_{neg}, and OD_{pos} are the absorbance values of the test sample, negative control (saline) and positive control (water), respectively. All the hemolysis experiments were done in triplicate.

WHOLE BLOOD CELL ATTACHMENT

Fresh blood collected from a healthy rabbit was mixed immediately with a 3.8 wt.% solution of sodium citrate at a dilution ration of 9:1. Neat and modified PP films of pieces (1 cm×1 cm) were incubated for 2 h in PBS and placed in a tissue culture plate. Then 2 mL of fresh whole blood was placed on the substrate surface in each well of the tissue culture plate for 60 min at 37℃. After the films were washed with PBS, blood cells adhering to the film were fixed by 2.5 wt. % glutaraldehyde at 4℃ for 10 h. Finally, the films were washed with PBS three times, and dehydrated with a series of ethanol/water mixtures (30, 50, 70, 90, and 100 vol. % ethanol; 30 min in each mixture). The surface of the film was gold sputtered in vacuum and observed with field emission scanning electron microscopy (SEM, FESEM, XL 30 ESEM FEG, FEI Company).

2.6 Blood Clotting Test

Fresh blood collected from a healthy rabbit was mixed immediately with a 3.8 wt.% solution of sodium citrate at a dilution ration of 9:1. The blood was centrifuged at 1000 rpm for 15 min to obtain the platelet-rich plasma (PRP). The films of pieces (1 cm×1 cm) were incubated for 2 h in PBS and placed in a tissue culture plate. Then 50 μL of fresh platelet rich plasma was dropped onto the center of the film and incubated at 37℃ for 60 min. The non-adhered platelets were rinsed by PBS for three times. Subsequently, the platelet adhering to the film was fixed by 2.5 wt.% glutaraldehyde at 4℃ for 10 h. Finally, the films were washed with PBS three times, and dehydrated with a series of ethanol/water mixtures (30, 50, 70, 90, and 100 vol. % ethanol; 30 min in each mixture), and then dried under vacuum. The surface of the film was gold sputtered in vacuum and observed with field emission scanning electron microscopy (FESEM, XL 30 ESEM FEG, FEI Company). The protein adsorption tests using a micro BCA^{TM} protein assay reagent kit (AR0146, Boster Biological Technology, Co., Ltd. Wuhan, China) and fluorescein isothiocynate-conjugated Fibrinogen (FITC-Fib) were presented in supporting information.

3. Results and Discussion

3.1 Immobilization of ATRP initiator on PP surface

For the preparation of polymer brushes, initiators immobilized on the PP film surface is indispensable. The procedure followed for the immobilization of ATRP initiator on the PP film is shown in Scheme 1. Neat PP films were first irradiated by oxygen plasma for 120 s to form hydroxide (-OH) at the outermost surface of PP. Then the PP-OH surface produced a stable initiator layer via the C-O-Si bonds. The chemical composition of the PP surface at various stages of surface was determined by XPS. Fig. 1a and 1b show the wide-scan spectra

of the neat PP and PP-CTPS. The appearance of the Si and Cl signals in the wide-scan spectrum of the PP-CPTS surface in
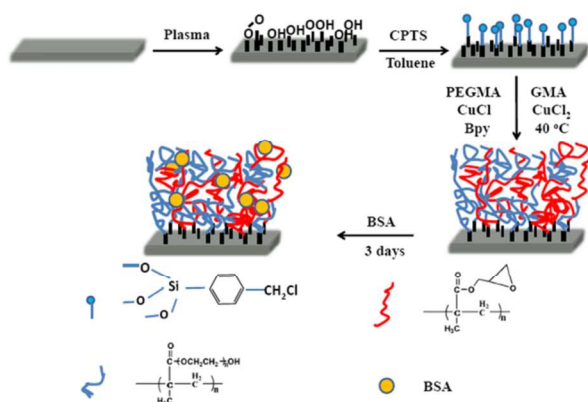
Scheme1. Schematic diagram illustrates the processes of BSA immobilization onto PP surface.

Fig. 1b showed the CPTS was immobilized on PP surface successfully. Parts c and d of Fig. 1 show the respective Si 2p and Cl 2p core level spectra of the PP-CPTS surface. The Cl 2p core-level spectrum was fitted with the Cl $2p_{3/2}$ and Cl $2p_{1/2}$ peak components at the BEs of about 200.0 and 201.6 eV respectively, attributable to the covalently bonded chlorine species of the benzyl chloride moiety of the immobilized silane. In order to estimate the ATRP initiator (benzyl chloride) density on the CPTS modified PP surface, the initiator density is firstly set as an unknown value, ρ^* (Cl /nm^2). Based on the initiator density (ρ^*), mass density (ρ_1) of the CPTS layer (1.1 g/cm^3)[26], and molecular weight (M_1) of CPTS (154 g/mol, excluding the 3 Cl atoms), the thickness (h) of the initiator layer was estimated to be about (h=$\rho^* \times M_1/\rho_1$). From the mass density (ρ_2) of the PP film (0.9 g/cm^3), the molecular weight (M_2) of the propylene repeat unit (36 g/mol), the stoichiometry (C_3H_3) of the propylene repeat unit, and the sampling depth (about 7.5 nm in an organic matrix[29]) of the XPS technique, the number (n) of the total C atoms per unit volume of the XPS probing depth (V = 7.5 nm^3) is about (290.25-2.2ρ^*) (6ρ^*+3(7.5-h)ρ_2/M_2)[30]. Based on the [Cl]/[C] ratio (r) of 4.4×10^{-2} (determined from the

sensitivity factor-corrected Cl 2p and C 1s core-level spectral area ratio of the PP-CPTS surface), the initiator density (ρ^*) for the PP-CPTS surface is estimated to be about 11.64 initiators/nm^2 (r=ρ^*/n). This value is much higher than the initiator density introduced with typical ATRP initiators by conventional methods (1-2 initiators/nm^2)[31, 32]. The significantly higher initiator density was good for effective density of protective layer for protein and cells.

3.2 Surface-Initiated ATRP of PEGMA and GMA on PP surface

GMA and hydrophilic monomer PEGMA were co-grafted onto PP film via SI-ATRP. This mixture of PEG-rich monomers and epoxy-containing GMA monomers allows us to control the non-fouling ability as well as BSA conjugation sites. At the initial stage of ATRP, a sufficient concentration of the deactivating Cu(II) complex is necessary to quickly establish an equilibrium between the dormant and active chains[33, 34]. In this study, the ratio of [PEGMA]: [CuCl]: [CuCl$_2$]: [Bpy] was controlled at 100:1:0.2:2.

In this work, the grafting density (GD) is defined as $GD=(W_m-W_0)/S$, where W_0 and W_m are the weights of the dry film before and after graft copolymerization, respectively, and S is the film area. The kinetics of the grafting reaction was studied and an approximately linear relation between grafting density and reaction times of P (PEGMA-co-GMA) chains was observed (Fig. 2). This result showed that the growth of polymer brushes from the PP-CPTS surface was a controlled and well-defined process.

The surface structure compositions of modified PP were confirmed by ATR-FTIR and XPS. Fig. 3 shows ATR-FTIR spectra of neat PP and PP modified with PEGMA and GMA. A new peak appeared at 1730 cm^{-1} in the spectra of PP-g-P (PEGMA-co-GMA), which was assigned to C=O stretching vibration in PEGMA or GMA. The intensities of the carbonyl group peaks increased with grafting time. The additional broad band in the range of 3000 cm^{-1} to 3600 cm^{-1} was assigned to characteristic -OH stretching of PEGMA. The comonomers PEGMA and GMA are difficult to distinguish. The
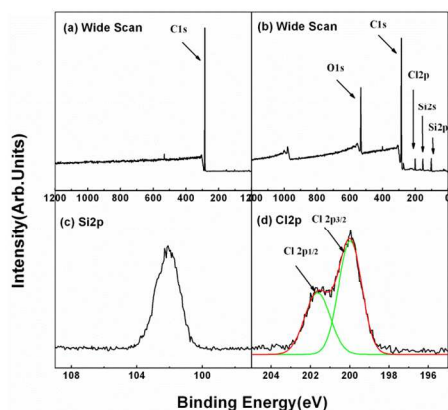

Fig. 1 Wide scan spectra of (a) PP and (b) PP-CPTS surface and Si 2p and Cl 2p core-level spectra of the (c and d) PP-CPTS surface.
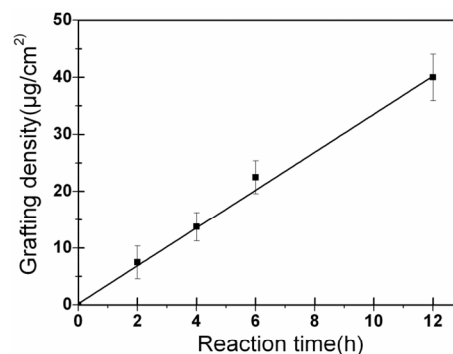

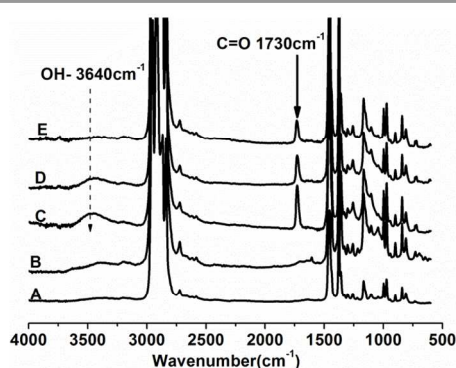Fig. 2 Dependence of the grafting density of the P(GMA and PEGMA) onto PP surface on ATRP reaction

Fig. 3 ATR-FTIR spectra of (A) neat PP, (B) PP-CPTS, (C) PP-g-P (PEGMA-*co*-GMA), (D) PP-g-P (PEGMA), (E) PP-g-P (GMA).

subsequently immobilized BSA could prove that GMA was successfully grafted.

Fig. 4 shows the C1s core-level spectra of PP-g-P (PEGMA-*co*-GMA). The spectra can be curve-fitted into three-peak component. The three-peak components with BEs at about 284.6, 286.2, and 288.4 eV are attributed to the C-H, C-O(C-Cl), and O-C=O species, respectively. The reaction conditions for the surface-initiated ATRP and the resulting surface compositions are summarized in Table 1. The obtained ratio of [O=C-O]:[C-O] for PP-g-P(PEGMA-*co*-GMA) (*GD*=40 µg/cm^2) sample was 1:7.8 which is close to the theoretical ratio of P(PEGMA) (1:8.5) and higher than the theoretical ratio of P(GMA) (1:3). The mole ratio of P(PEGMA) and P(GMA) in polymer brushes can be estimated from the [O=C-O]:[C-O] vale. The P(PEGMA):P(GMA) was 6.9:1 for PP-g-P(PEGMA-*co*-GMA) (*GD*=40 µg/cm^2) sample. Besides, the intensity of the C-H species has decreased significantly with the increasing ATRP time. In a copper-mediated normal ATRP, the copper(I)/copper(II) salts used are toxic to human health and
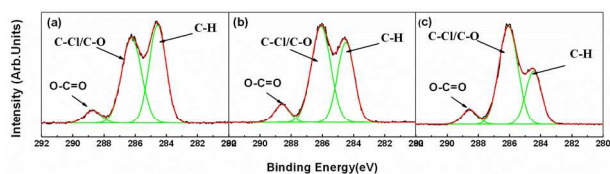
are difficult to remove completely from the products.[35]. For surface-initiated ATRP on the membrane, the copper(I)/copper(II) salts absorbed on the membrane was easy to removed by washing. The XPS wide scan spectra data of PP-g-P (PEGMA-*co*-GMA) confirmed that there was no copper on the membrane surface. These results confirmed that PEGMA and GMA were co-grafted onto the surface of PP surface.

On the basis of the average cross-sectional area (about 2 nm^2) of methacrylate polymers grafted by controlled radical polymerizations[30], the initiator density (ρ*) of 11.64 initiators/nm^2, the surface initiator efficiency e ($e = 1/(2\rho*)$) of the investigated PP-CPTS surface is estimated to be about 4.30 %. Note that the initiation efficiency cannot be reliably estimated, because the actual initiation efficiency will be dependent very much on the monomer type, reaction conditions and reactivity, and molecular weight of the grafted polymer[30]. Chain termination by bimolecular coupling or disproportionation reaction may have induced by the loss of the active chain ends (the terminal alkyl halides)[36, 37]. Besides, by taking into account of the molecular weight of PEGMA (360 g/mol) and GMA (142.15 g/mol), *GD* of P(PEGMA-*co*-GMA) brushes and P(PEGMA): P(GMA), the corresponding values of average degrees of polymerization (DP=*GD*/(Mρ*e) for PP-g-P(PEGMA-*co*-GMA) (*GD*=40 µg/cm^2) should be 1598.

The surface morphologies of the grafted films were studied by SEM and AFM. Fig. 5 shows the cross-sectional images of the PP-g-P(PEGMA-*co*-GMA). The new polymer layer appeared and the uniformly grafted P(PEGMA-*co*-GMA) polymers were well formed on the PP film surface. Additionally, it was clearly seen that the thickness of the film from ATRP time of 12 h was up to 140 to 150 nm. The changes in surface topography of the PP films after modified were investigated by AFM (Fig. 6). The PP film surface was rather uniform with a RMS of about 2.07 nm (Fig. 6a). After subsequent graft polymerization, obvious changes in surface morphologies of the PP-g-P(PEGMA-*co*-GMA) were observed. The RMS values of the PP-g-P(PEGMA-*co*-GMA) increased to be about 4.84 nm with *GD* of 40.0 nm (Fig. 6d). The increase in surface roughness of the modified surface was caused by the formation of the brushes on the surface. The above results also clearly confirmed that the dense P(PEGMA-*co*-GMA) brushes were readily grafted onto the PP surfaces.

The hydrophilicity of neat and modified PP films was investigated by water contact angles. Fig. 7 shows the water

Fig. 4 Wide scan and C 1s core-level spectra of PP-g-P (PEGMA-co-GMA) of GD of (a) 7.5 µg/cm^2, (b) 13.8 µg/cm^2 and (c) 40.0 µg/cm^2.

Table 1. ATRP reaction time, grafting density, chemical composition for the PP sample surfaces

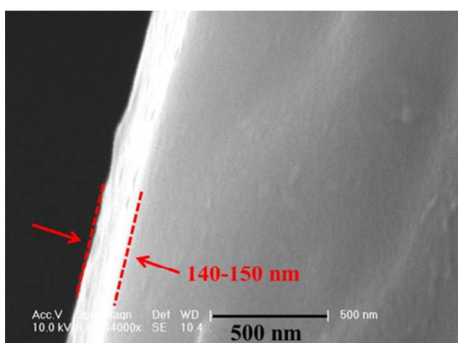| samples	Reaction time	Grafting density(µg/cm^2)	[O=C-O]/[C-O]	Cl/C
PP	-	-	-	-
PP-Plasma	120 s	-	-	-
PP-CPTS	2 h	-	-	4.4×10^{-2}
PP-g-P(PEGMA-co-GMA)	2 h	7.5 ± 2.9	1:4.5	2.5×10^{-2}
PP-g-P(PEGMA-co-GMA)	4 h	13.8 ± 2.5	1:7.7	9.5×10^{-3}
PP-g-P(PEGMA-co-GMA)	12 h	40.0 ± 4.1	1:7.8	1.8×10^{-3}

Fig. 5. SEM images of the cross-sectional views of PP-g-P(PEGMA-*co*-GMA) with GD = 40.0 µg/cm^2.

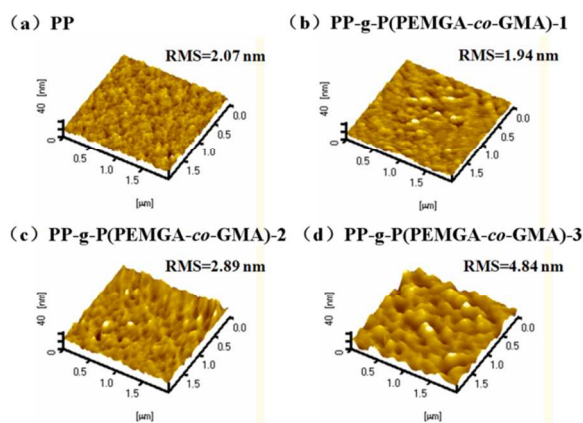**Fig. 6** AFM three-dimensional images of the (a) neat PP, (b, c, and d) PP-g-P(PEGMA-*co*-GMA) with GD of 7.5, 13.8 and 40.0 µg/cm^2.
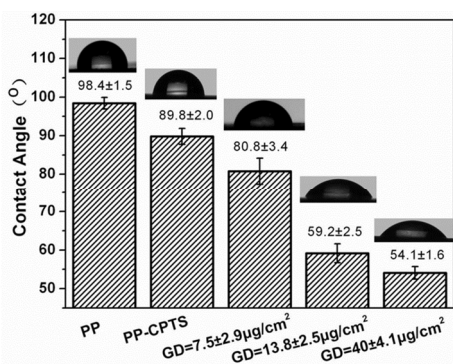

Fig. 7 Water contact angle of neat PP surface, PP-CPTS and PP-g- P(PEGMA-*co*-GMA) with different grafting density.

contact angles of neat and modified PP films. The neat PP film had the water contact angle around 98°, indicating its high

hydrophobicity. The ATRP initiator immobilized PP film had a pronounced surface hydrophobicity, with a water contact angle of 90°. After polymerization, the contact angle decreased to 54°, indicating that the surface of the modified PP films became hydrophilic because of the introduction of PEGMA. The water contact angle of the modified PP further decreased with increasing graft density. The results indicate that the
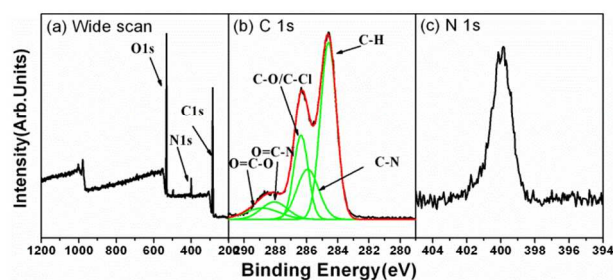

Fig. 8 XPS spectra of BSA modified PP film surface (a) Wide scan, (b) C 1s and (c) N 1s (GD = 40 µg/cm^2).
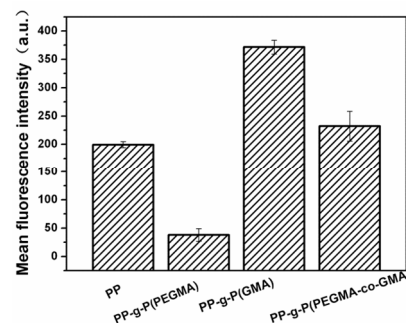

Fig. 9 Fluorescence intensity of FITC-BSA immobilized onto neat PP, PP-g-P (PEGMA), PP-g-P (GMA) and PP-g-P (PEGMA-*co*-GMA).

hydrophilicity of PP films is improved after modification with PEGMA and GMA. As the consequence, the method here proposed for SI-ATRP on the PP surface is usefully applicable to other polyolefin.

3.3 Immobilization of BSA

The epoxide group of PP-g-P (PEGMA-*co*-GMA) films can react feasibly and irreversibly with nucleophilic groups such as amino-, carboxyl-, and sulfhydryl-. Thus, the epoxide group on the modified PP surface was well suited for immobilization of BSA with the abundant amount amino groups. P (PEGMA) ensured the blood compatibility and the activity of immobilized BSA. ATR-FTIR (Fig. S1) and FT-IR microscopy (Fig. S2) were employed to characterize the surface composition of PP-g-P(PEGMA-*co*-GMA)-g-BSA films. XPS was employed to investigate the detailed chemical composition of PP-g-P (PEGMA-*co*-GMA)-g-BSA film, as shown in Fig. 8. Both neat PP and PP-g-P(PEGMA-*co*-GMA) films had no nitrogen signal, but a nitrogen signal was obviously present on the BSA modified films(Fig. 8a). The C1s peak of the BSA modified film in Fig. 8 b also fitted with five-peak components. Two more peaks were found at 288.0 and 285.9 eV, which are attributed to O=C-N and C-N species, respectively. Based on the only source of elemental N in the BSA macromolecule, N can be used to calculate the degree of BSA surface coverage (Γ_{BSA}) on the film surface with the following equation[7, 38].

$$\Gamma_{BSA} = \frac{A_{mN}}{A_{pN}} \times 100\%$$

where A_{mN} is the nitrogen atomic percentage on the PP film surface measured by XPS, and A_{pN} is the nitrogen atomic percentage of BSA under complete coverage of the membrane surface with BSA. A_{pN} is 12.95% based on the total atomic composition of C, O, N and S elements in pure BSA powder. The BSA surface coverage degree is 19.4%. All these results confirmed that BSA was successfully immobilized onto the surface of PP film.

To visualize the BSA immobilization, fluorescein isothiocynate-conjugated BSA (FITC-BSA) was immobilized onto the surface of PP coupled with different monomers[8, 39]. The fluorescence intensity is proportional to the density of FITC-BSA on the surface[40]. Fig. 9 shows the corresponding fluorescence intensity of neat and modified PP films. The fluorescence of neat PP was due to the adsorption of FITC-BSA on the surface. This phenomenon corresponded to the protein adsorption test, which was discussed in supporting information. Fluorescence intensity was hardly observed on the PEGMA modified PP films because of the protein resistance of PEG. By contrast, intense fluorescence intensity was observed across the GMA modified PP surface, which demonstrated a large amount of FITC-BSA on the surface. The abundant FITC-BSA on the GMA modified surface was the result of two events, namely, physical adsorption and covalent binding. The fluorescence intensity of PP-g-P (PEGMA-*co*-GMA) film was between the intensities of PEGMA modified and GMA modified PP surfaces. PEGMA could inhibit non-specific BSA adsorption, whereas GMA could covalently immobilize BSA by ring-open reaction of the epoxy group. The balance of these two interactions caused the moderate fluorescence intensity.

BSA is the most widely utilized serum protein due to its wide availability, low cost, and structural/functional similarity to human serum albumin—with 76% sequence homology and nearly identical pH-dependent conformational transitions. Some researchers[41, 42] found that BSA adsorption on materials reached a maximum at isoelectric point pH 4.7 because of the minimum conformational alteration of BSA and energy loss. However, few studies have been conducted on the influence of pH on BSA immobilization onto biomaterial surfaces. To

confirm the influence of pH on BSA immobilization, BSA was immobilized in buffers with different pH solution conditions at 2.5, 4.7 and 7.4. The XPS spectra of the BSA-modified film surfaces with different pH solution conditions are presented in Fig. 10. The N/C was was also given in Fig. 10. The maximum value of immobilization capacity was achieved at pH 7.4 which was the same as the physiological conditions. The reason may be attributed to the different conformations of the BSA molecule in different pH solutions when the epoxide group on the PP surface reacts with BSA. The disulfide bridges provide the basis for the compact heart-shaped (equilateral triangle) structure (the donated N form)[43], which is proposed for BSA in the pH range of 4.5 to 8 as well as the stability to the helical structure. Below pH 4.5, a reversible unfolding occurs that results in the so-called fast form (F form), which possesses more reduced solubility, elongated shape, and increased viscosity[44, 45]. The reduced solubility and increased viscosity caused difficulties in the reaction of BSA with the epoxide group on PP surface. Therefore, in pH 7.4 solutions, more amino groups in BSA could react with the epoxy on the surface of the modified PP, which results in the maximum value of immobilization capacity. Another reason was that higher pH facilitated coupling efficiency because of highly pH-dependent reactivity of the epoxy group.

3.4 Hemolysis test

HEMOLYSIS RATE

Hemolysis rate is an important parameter for evaluating blood compatibility[46, 47]. The ratio represents the extent of the RBC rupture caused by the release of Hb. The anticoagulant performance of PP-based biomaterials had been extensively studied, but the research on biomaterial surface-induced hemolysis is significantly neglected, especially hemolysis during RBCs storage and transportation. For the BSA modified PP, we focused on hemolysis rate quantitatively and on whole blood cell adhesion qualitatively to reveal the interactions between RBCs and the PP surface. The hemolysis ratios of neat and modified PP are shown in Fig. 11. The hemolysis rates of the modified films are lower than that of neat PP. The hemolysis rate decreased as the grafting density increased from 22.5 and 40.0 $\mu g/cm^2$ (Fig. 11b and c). The hemoylsis rate of different molar ration of monomer modified PP was also investigated (Fig. S3). When hydrophobic PP was exposed to blood, the ductility and maximal stress of RBC would be induced by some modes, which then resulted in the release of Hb and the rupture of the RBC membrane[48]. PEGMA modified surface could reduce the RBC membrane maximal stress due to its hydrophilicity. The hemolysis rate of the BSA-modified PP film was lower than the corresponding PP-g-P (PEGMA-*co*-GMA). This result was consistent with the research by Poonam Khullar[22]. The photos of hemolyisi test were shown in the insert figure in Fig. 11. The red solution indicated that the RBC was destroyed, and hemoglobin was released. There was nearly no hemolysis for negative control (-) and completely hemolysis for positive control (+). The hemolysis of PP sample could be seen from the color. The neat PP with large hemolysis exhibited
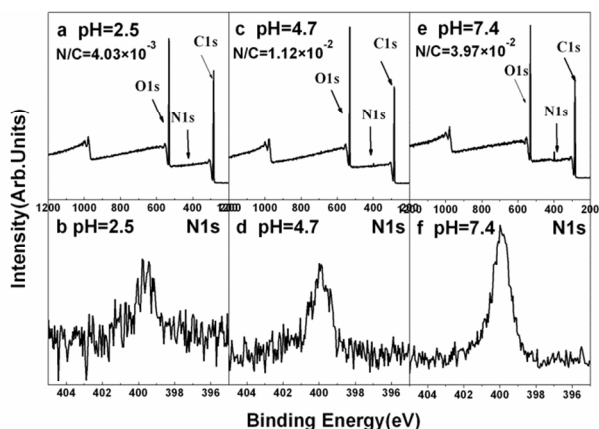

Fig. 10 XPS spectra and N/C values of BSA modified PP film surface with different pH at 2.5 (a and b), 4.7 (c and d) and 7.4 (e and f).
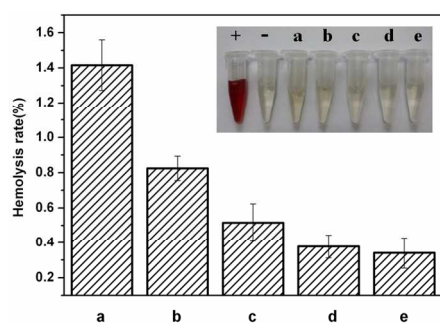
Fig. 11 Hemolysis test results of (a) neat PP films, (b and c) the PP-g-P(PEGMA-*co*-GMA) surface obtained at the grafting density of 22.5 and 40.0 μg/cm^2 and (d and e) BSA immobilization on the PP-g-P(PEGMA-*co*-GMA) obtained at the the grafting density of 22.5 and 40.0 μg/cm^2, where the hemolysis rate of the positive control (water) and negative control (saline) were 1 and 0, respectively. The inserted image showed the photos of hemolyisi test.

slightly dark color, whereas no obviously difference of the color for modified samples due to the low hemolysis. Besides, the hemolysis rate of BSA modified PP was lower than PEGMA modified PP films (Fig. S3). The decrease of the hemolysis rate of the BSA-modified film was primarily related to the presence of albumin proteins on the PP surface. Two main reasons are contributed to the lower hemolysis rate. First, PP films are partially passivated by the BSA coating. BSA coating can maintain the ductility and fragility of RBC, which leads to hemolysis. Second, the negative charge of BSA repels the approach of RBCs to the surface by electrostatic interactions. Under the conditions of physiological pH, the erythrocytes from numerous animal species have negative surface charge. The isoelectric point of BSA is pH 4.7. Therefore BSA also has a negative charge under the conditions of physiological pH. The BSA-modified PP consequently presents remarkable anti-hemolysis owing to the hydrophilicity and surface well-distributed negative charges of BSA. Therefore, BSA could decrease the hemolysis rate of PP given the inertness and negative charge of BSA. Red blood cell membrane maximal stress can be reduced by the hydrophilicity of BSA as well as the repulsion caused by its electrostatic interactions.

Whole blood cells attachment

Stable hemocompatibility of biomedical membranes used in contact with human whole blood is highly desirable for hemodialysis devices or blood filters[49]. In general, a multistep process of plasma protein adsorption, blood platelet adhesion, and blood cell attachment strongly affects the different stages of thrombotic response induced by the blood-contacting membranes[50]. Upon the first contact of blood with a biomaterials surface, proteins adsorb to form a conditioning film to which platelets adhere. After adhesion, platelets will spread and start degranulation. Granule constituents, such as adenosinediphosphate (ADP), and products of the arachidonic acid metabolism will activate and recruit other platelets, resulting in a growing platelet aggregate. Adhering platelets also express activated membrane structures, such as glycoprotein IIb-IIIa (GpIIb-IIIa) complex and
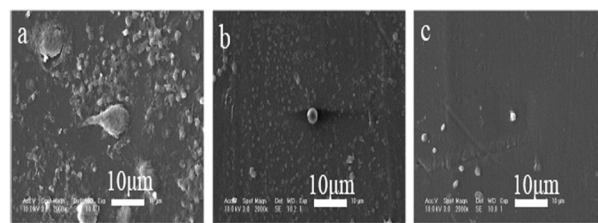

Fig. 12 SEM images of whole blood cells adhered onto the surface of (a) neat PP films, (b) the PP-g-P (PEGMA-*co*-GMA) surface (c) the BSA modified PP film surface (GD = 40.0 μg/cm^2).

phosphatidylserine. The above events ultimately lead to the formation of thrombi on the biomaterials surface and in blood[51]. Whole blood cells adhesion can reveal the all-around performance of a PP-based biomaterial when exposed to the complex blood compositions, including plasma proteins, platelets, leukocytes, RBCs. As shown in Fig. 12, the surface of the PP films was densely covered with platelets, leukocytes, RBCs, and fibrin networks. Spread, activated platelets and leukocytes were observed. Medium-size thrombi (Fig. 12a), containing RBCs and fibrin networks were also found because the high hydrophobicity of PP-induced blood cells inactivation. By contrast, Fig. 12b and Fig. 12c showed that platelet activation and thrombosis formation (RBC rupture and adhesion) were remarkably suppressed on the modified PP films. The suppressed whole blood cell attachment can also be explained by the mobility or flexibility of highly hydrated chains, the large, excluded volume of PEG units in the water and the partially passivation by BSA. As a result, the hemocompatibility of the modified PP films was ameliorated and BSA molecules weakened the interaction between blood cells and the PP surface.

3.5 Platelet adhesion

Once plasma protein is adsorbed on the surface of a biomaterial, platelets adhere, spread and aggregate[51], which ultimately led to thrombus formation. Surface wettability and plasma protein adsorption can affect the amount of platelet transmutation on the surface[52, 53]. Fig. 13 shows the platelet adhesion on the surface of neat and modified PP. A large amount of platelets adhered on neat PP film surface (Fig. 13a), exhibiting a high aggregation degree. The platelets were highly activated with spread, aggregation and pseudopodia states, because the platelet adhesion was controlled by protein adsorption, especially fibrinogen (Fib). Neat PP film had the highest Fib adsorbed amount because of its high hydrophobic property (Fig. S6 and
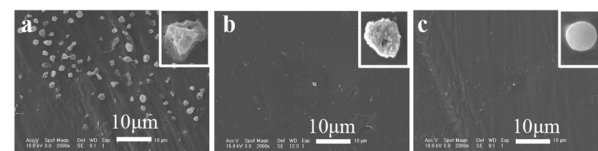

Fig. 13 SEM images of platelet adhered on the surface of (a) neat PP film, (b) the PP-g-P (PEGMA-*co*-GMA) surface (c) the BSA modified PP film surface (GD = 40.0 μg/cm^2).

S7). Hydrophobicity could induce some conformational change in Fib, which exposed hidden sites in Fib that could be recognized by platelet receptors[52]. In Fig. 13b, nearly no platelet adhered on the surface of PP-g-P(PEGMA-*co*-GMA) with the grafting density of 40 μg/cm^2. Fib adsorption was suppressed by the modification of PEGMA. The hydrophilicity of PEGMA can maintain the native conformational of the adsorbed Fib. In addition, the steric hindrance effect of PEGMA could prevent the platelet adhesion. The BSA-modified film also showed excellent anti-platelet adhesion properties (Fig. 13c). Although the amount of Fib adsorbed on the BSA-modified PP is higher than PEGMA modified PP (Fig. S4), no transmutative platelet adhered on the surface of the BSA-modified PP. This result could be attributed to the fact that the inertness of BSA could inhibit the conformational changes. Balakrishnan Sivaraman[54] found that the degree of structural unfolding of the adsorbed Fib is the much greater determinant of the platelet response than the amount of Fib adsorbed. Therefore, BSA modified PP could suppress platelet adhesion by inhibiting transformation of Fib in plasma to fibronectin.

4. Conclusions

In this study, BSA surface-immobilization onto PP was used to decrease the hemolysis of the films, which was the essential issue in biomaterials used for blood storage and transportation. The ATRP initiator CPTS was immobilized after plasma pretreatment, and then PP-g-P (PEGMA-*co*-GMA) film was fabricated via SI-ATRP of PEGMA and GMA. Kinetics study confirmed the controlled feature of SI-ATRP. PEGMA chain was used to inhibit non-specific protein adsorption, and GMA was used to covalently immobilize BSA by the ring-open reaction of the epoxy group. The modified PP films were characterized by ATR-FTIR, XPS. The maximum BSA immobilization capacity was achieved at pH 7.4. Hemolysis test showed that BSA could decrease the hemolysis rate of PP because of its inertness and negative charge. Moreover, the whole blood cell attachment test showed that the BSA-modified films remarkably suppressed platelet activation and thrombosis formation. Thus, the immobilization of BSA on PP films with PEGMA and GMA as spacer is an effective way to improve the antihemolytic properties of PP. The method proposed here for BSA immobilization on the PP surface can also be applicable to immobilize other functional biomolecules such as antibody on polymeric platform with excellent hemocompatibility.

Acknowledgements

Note and References

1   S. Deutsch, J. M. Tarbell, K. B. Manning, G. Rosenberg and A. A. Fontaine, *Annual Review of Fluid Mechanics*, 2006, **38**, 65-86.

2   H. Hu, X. B. Wang, S. L. Xu, W. T. Yang, F. J. Xu, J. Shen and C. Mao, *J. Mater. Chem.*, 2012, **22**, 15362-15369.

3   S. Mansouri, Y. Merhi, F. o. M. Winnik and M. Tabrizian, *Biomacromolecules*, 2011, **12**, 585-592.

4   C. Stoll and W. F. Wolkers, *Transfus. Med. Hemother.*, 2011, **38**, 89-97.

5   L. R. Montes, D. J. López, J. s. Sot, L. A. Bagatolli, M. J. Stonehouse, M. L. Vasil, B. X. Wu, Y. A. Hannun, F. l. M. Goñi and A. Alonso, *Biochemistry (Mosc.)*, 2008, **47**, 11222-11230.

6   J. Jin, W. Jiang, Q. Shi, J. Zhao, J. H. Yin and P. Stagnaro, *Appl. Surf. Sci.*, 2012, **258**, 5841-5849.

7   C. Zhang, J. Jin, J. Zhao, W. Jiang and J. Yin, *Colloids and Surfaces B: Biointerfaces*, 2013, **102**, 45-52.

8   K. K. Goli, O. J. Rojas and J. Genzer, *Biomacromolecules*, 2012, **13**, 3769–3779.

9   K. K. Goli, N. Gera, X. Liu, B. M. Rao, O. J. Rojas and J. Genzer, *ACS Appl. Mater. Interfaces*, 2013, **5**, 5298-5306.

10   K. K. Goli, O. J. Rojas, A. E. Özçam and J. Genzer, *Biomacromolecules*, 2012, **13**, 1371-1382.

11   S. Yuan, G. Xiong, A. Roguin and C. Choong, *Biointerphases*, 2012, **7**, 1-12.

12   F. He, B. Luo, S. Yuan, B. Liang, C. Choong and S. O. Pehkonen, *RSC Advances*, 2014, **4**, 105-117.

13   T. Riedel, Z. Riedelová-Reicheltová, P. Májek, C. Rodriguez-Emmenegger, M. Houska, J. E. Dyr and E. Brynda, *Langmuir*, 2013, **29**, 3388–3397.

14   Z. Zhou, P. Yu, H. M. Geller and C. K. Ober, *Biomacromolecules*, 2013, **14**, 529–537.

15   F. A. Rahim and K. Dong-Hwan, *RSC Advances*, 2013, **3**, 9785-9793.

16   C. J. Fristrup, K. Jankova, R. Eskimergen, J. T. Bukrinsky and S. Hvilsted, *Polymer Chemistry*, 2012, **3**, 198-203.

17   Y.-L. Liu, C.-C. Han, T.-C. Wei and Y. Chang, *Journal of Polymer Science Part A: Polymer Chemistry*, 2010, **48**, 2076-2083.

18   Z. Liu, X. Deng, M. Wang, J. Chen, A. Zhang, Z. Gu and C. Zhao, *J. Biomater. Sci. Polym. Ed.*, 2009, **20**, 377-397.

19   B. H. Fang, Q. Y. Ling, W. F. Zhao, Y. L. Ma, P. L. Bai, Q. Wei, H. F. Li and C. S. Zhao, *J. Membr. Sci.*, 2009, **329**, 46-55.

20   A. He, B. Lei, C. Cheng, S. Li, L. Ma, S. Sun and C. Zhao, *RSC Advances*, 2013, **3**, 22120-22129.

21   G. Barshtein, D. Arbell and S. Yedgar, *IEEE Trans. Nanobioscience*, 2011, **10**, 259-261.

22   P. Khullar, V. Singh, A. Mahal, P. N. Dave, S. Thakur, G. Kaur, J. Singh, S. Singh Kamboj and M. Singh Bakshi, *The Journal of Physical Chemistry C*, 2012, **116**, 8834-8843.

23   W. Hu, Y. Liu, Z. Lu and C. M. Li, *Adv. Funct. Mater.*, 2010, **20**, 3497-3503.

24   Y. Liu, W. Wang, W. Hu, Z. Lu, X. Zhou and C. M. Li, *Biomedical microdevices*, 2011, **13**, 769-777.

25   Y. Liu, C. X. Guo, W. Hu, Z. Lu and C. M. Li, *J. Colloid Interface Sci.*, 2011, **360**, 593-599.

26   F. Zhang, F. J. Xu, E. T. Kang and K. G. Neoh, *Ind. Eng. Chem. Res.*, 2006, **45**, 3067-3073.

27   F. J. Xu, E. T. Kang and K. G. Neoh, *Macromolecules*, 2005, **38**, 1573-1580.

28   F. J. Xu, S. P. Zhong, L. Y. L. Yung, E. T. Kang and K. G. Neoh, *Biomacromolecules*, 2004, **5**, 2392-2403.

29 K. L. Tan, L. L. Woon, H. K. Wong, E. T. Kang and K. G. Neoh, *Macromolecules*, 1993, **26**, 2832-2836.

30 F. J. Xu, J. P. Zhao, E. T. Kang and K. G. Neoh, *Ind. Eng. Chem. Res.*, 2007, **46**, 4866-4873.

31 H. Jiang, X. B. Wang, C. Y. Li, J. S. Li, F. J. Xu, C. Mao, W. T. Yang and J. Shen, *Langmuir*, 2011, **27**, 11575-11581.

32 J. Hou, Q. Shi, P. Stagnaro, W. Ye, J. Jin, L. Conzatti and J. Yin, *Colloids and Surfaces B: Biointerfaces*, 2013, **111**, 333-341.

33 K. Matyjaszewski, P. J. Miller, N. Shukla, B. Immaraporn, A. Gelman, B. B. Luokala, T. M. Siclovan, G. Kickelbick, T. Vallant, H. Hoffmann and T. Pakula, *Macromolecules*, 1999, **32**, 8716-8724.

34 F. J. Xu, D. Xu, E. T. Kang and K. G. Neoh, *J. Mater. Chem.*, 2004, **14**, 2674-2682.

35 F. Tang, L. Zhang, J. Zhu, Z. Cheng and X. Zhu, *Ind. Eng. Chem. Res.*, 2009, **48**, 6216-6223.

36 F. J. Xu, Z. L. Yuan, E. T. Kang and K. G. Neoh, *Langmuir*, 2004, **20**, 8200-8208.

37 F. J. Xu, Y. L. Li, E. T. Kang and K. G. Neoh, *Biomacromolecules*, 2005, **6**, 1759-1768.

38 J. Zhao, Q. A. Shi, S. F. Luan, L. J. Song, H. W. Yang, H. C. Shi, J. Jin, X. L. Li, J. H. Yin and P. Stagnaro, *J. Membr. Sci.*, 2011, **369**, 5-12.

39 S. Yuan, D. Wan, B. Liang, S. O. Pehkonen, Y. P. Ting, K. G. Neoh and E. T. Kang, *Langmuir*, 2011, **27**, 2761-2774.

40 F. Darain, K. Gan and S. Tjin, *Biomed Microdevices*, 2009, **11**, 653-661.

41 Z. G. Peng, K. Hidajat and M. S. Uddin, *J. Colloid Interface Sci.*, 2004, **271**, 277-283.

42 W. K. Li and S. J. Li, *Colloid Surf. A-Physicochem. Eng. Asp.*, 2007, **295**, 159-164.

43 D. C. Carter and J. X. Ho, in *Adv. Protein Chem.*, eds. J. T. E. F. M. R. C.B. Anfinsen and S. E. David, Academic Press, 1994, vol. 45, pp. 153-203.

44 M. Y. Khan, *Biochem. J.*, 1986, **236**, 307-310.

45 D. H. Tsai, F. W. Delrio, A. M. Keene, K. M. Tyner, R. I. Maccuspie, T. J. Cho, M. R. Zachariah and V. A. Hackley, *Langmuir*, 2011, **27**, 2464–2477.

46 J. P. Singhal and A. R. Ray, *Biomaterials*, 2002, **23**, 1139-1145.

47 H. Jiang, X. B. Wang, C. Y. Li, J. S. Li, F. J. Xu, C. Mao, W. T. Yang and J. Shen, *Langmuir*, 2011, **27**, 11575-11581.

48 C. Cheng, S. Li, S. Nie, W. Zhao, H. Yang, S. Sun and C. Zhao, *Biomacromolecules*, 2012, **13**, 4236-4246.

49 B. D. Ratner, *Biomaterials*, 2007, **28**, 5144-5147.

50 S. H. Chen, Y. Chang, K. R. Lee, T. C. Wei, A. Higuchi, F. M. Ho, C. C. Tsou, H. T. Ho and J. Y. Lai, *Langmuir*, 2012, **28**, 17733-17742.

51 H. T. Spijker, R. Bos, H. J. Busscher, T. G. van Kooten and W. van Oeveren, *Biomaterials*, 2002, **23**, 757-766.

52 B. Sivaraman and R. A. Latour, *Biomaterials*, 2010, **31**, 832-839.

53 P. Yang, N. Huang, Y. X. Leng, J. Y. Chen, R. K. Y. Fu, S. C. H. Kwok, Y. Leng and P. K. Chu, *Biomaterials*, 2003, **24**, 2821-2829.

54 B. Sivaraman and R. A. Latour, *Biomaterials*, 2010, **31**, 832-839.

[a] State Key Laboratory of Polymer Physics and Chemistry, Changchun Institute of Applied Chemistry, Chinese Academy of Sciences, Changchun 130022, PR China. E-mail: jjin@ciac.ac.cn; yinjh@ciac.ac.cn; Fax: +86-431-85262126; Tel: +86-431-85262971

[b] Graduate University of Chinese Academy of Sciences, Beijing 100049, PR China.

[c] Polymer Materials Research Center, College of Materials Science and Chemical Engineering, Harbin Engineering University, Harbin 150001, PR China.
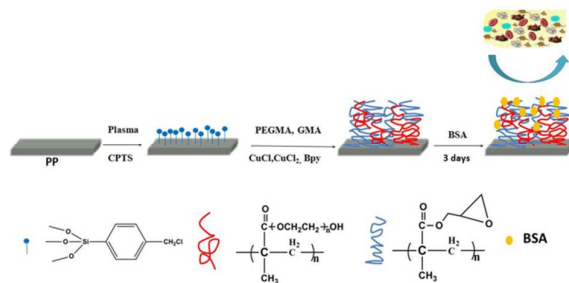
Bovine serum albumin modified polypropylene for hemocompatibility was fabricated via surface-initiated atom transfer radical polymerization.